

Quasi-one Dimensional Nanostructures as Sign of Nematicity in Iron Pnictides and Chalcogenides

Dheeraj Kumar Singh^{1,2,3,*}, Alireza Akbari^{2,3,4,†} and Pinaki Majumdar¹

¹*Harish-Chandra Research Institute, HBNI, Chhatnag Road, Jhansi, Allahabad 211019, India*

²*Asia Pacific Center for Theoretical Physics, Pohang, Gyeongbuk 790-784, Korea*

³*Department of Physics, POSTECH, Pohang, Gyeongbuk 790-784, Korea and*

⁴*Max Planck POSTECH/Korea Research Initiative (MPK), Gyeongbuk 376-73, Korea*

(Dated: March 1, 2022)

Impurity scattering is found to lead to quasi-one dimensional nanoscale modulation of the local density of states in the iron pnictides and chalcogenides. This ‘quasiparticle interference’ feature is remarkably similar across a wide variety of pnictide and chalcogenide phases, suggesting a common origin. We show that a unified understanding of the experiments can be obtained by simply invoking a four-fold symmetry breaking $d_{xz} - d_{yz}$ orbital splitting, of a magnitude already suggested by the experiments. This can explain the one-dimensional characteristics in the local density of states observed in the orthorhombic nematic, tetragonal paramagnetic, as well as the spin-density wave and superconducting states in these materials.

The intriguing anisotropic electronic properties of iron pnictides [1] are reflected in transport measurements [2–4], optical conductivity [5], angle-resolved photoemission spectroscopy (ARPES) [6], and scanning tunneling microscopy (STM) [7]. It is not unexpected in a state having a broken four-fold rotational symmetry such as the spin-density wave (SDW) state or the orthorhombic ‘spin nematic’ state, but the lattice anisotropy does not explain the splitting of ≈ 60 meV between the d_{xz} and d_{yz} orbitals [8, 9]. The orbital splitting (OS) actually persists into the high temperature tetragonal phase [9]. This suggests that the OS, rather than the orthorhombic symmetry or magnetic order, could be the key player in electronic anisotropy. A similar OS exists in various phases [10–15] of the chalcogenide including the superconducting state. The energy scale of FeSe splitting, and its orbital character, has been contrasted with those of the pnictides, with some suggestions of a momentum dependent, *i.e.*, non-uniform splitting. Unlike the pnictides where the degeneracy of bands is dominated mainly by d_{xz} and d_{yz} orbitals at X or Y points is lifted at low temperature, the OS for chalcogenides may also exhibit sign reversal. Some have reported it to be of entirely different nature, OS between $d_{xz/yz}$ and d_{xy} [16, 17].

Valuable insight into electronic anisotropy can be obtained through the ‘quasiparticle interference’ (QPI) phenomena which basically probes the spatial variation of the local density of states (LDOS), due to impurities in the medium, using the spectroscopic imaging STM [18]. A remarkable characteristic of the QPI common to the SDW state, the orthorhombic nematic phase, and the tetragonal paramagnetic phase, in some of the pnictides is the occurrence of quasi-one dimensional real-space LDOS modulation with material dependent lengthscale [7, 19, 20]. Corresponding momentum-space structure in the form of almost parallel ridges are aligned along a direction reciprocal to the ferromagnetic direction in the SDW state, or *b*-axis in the orthorhombic phase for pnictides. Similar momentum- and real-space structures have been reported in superconducting phase of chalcogenides [11].

This suggests a common origin of the anisotropy in the electronic structure, rather than in specific ordering tendencies.

In the SDW state, the orbital occupancy difference that can result from the electronic reconstruction is $n_{xz} - n_{yz} \sim 0.1$ [21], which corresponds roughly to an energy splitting of 50 meV. According to the experiments, the OS observed above Neel temperature T_N can be as large as ~ 60 meV [6], therefore it is natural to explore the consequences of this ‘orbital bias’ in studying the SDW state as well, ignored in earlier work which may have led to their failure in reproducing the one dimensional (1d) characteristics with correct orientation and lengthscale [22–25]. Such a term should assume further importance, beyond magnetic anisotropy, in the electron-doped region of SDW state where the magnetic moments are small, and magnetic order induced band reconstruction is less pronounced.

Above T_N , a non-zero OS has been attributed to the spin-driven nematic order with $\langle \mathbf{S}_i \cdot \mathbf{S}_{i+x} - \mathbf{S}_i \cdot \mathbf{S}_{i+y} \rangle \neq 0$, where average magnetic moment $\langle \mathbf{S}_i \rangle = 0$, because of the frustration caused by the presence of second nearest-neighbor exchange coupling [26–28]. It is not clear enough how this mechanism will support OS term of similar strength below T_N in the SDW state, which we find necessary to explain the 1d QPI characteristics. In another scenario, OS may also originate from the ferro-orbital order [29–32] caused by the spin-orbital mode coupling, which can be responsible for an OS larger than what is expected merely induced by the SDW state. Behavior of orbital order appears to have a remarkable similarity to some of the manganites where the orbital order precedes the magnetic order as temperature is lowered [33] except that the lattice distortion is small enough in iron-based superconductors to account for such a large OS.

In this letter, we suggest a unified explanation for the common QPI characteristics of different phases of iron-based superconducting systems. Our proposal is that an explicit OS term in the Hamiltonian is crucial irrespective of phases. Thus, our point of departure in the standard five-orbital Hamiltonian is the OS term:

$$\mathcal{H}_{orb} = -\frac{\delta}{2} \sum_{i\sigma} (d_{ixz\sigma}^\dagger d_{ixz\sigma} - d_{iyz\sigma}^\dagger d_{iyz\sigma}). \quad (1)$$

Here, $d_{i\gamma\sigma}^\dagger$ ($d_{i\gamma\sigma}$) is the creation (annihilation) operator for an

* dheeraj@postech.ac.kr

† alireza@apctp.org

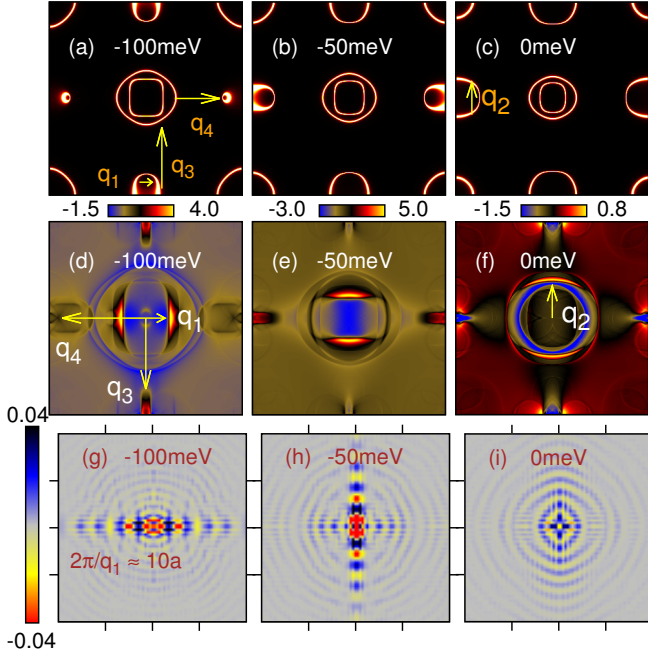


FIG. 1. Results in the nematic state for orbital splitting $\delta = 60$ meV: (a-c) show the behavior of contours of constant energies (CCEs) for the quasiparticle energy $\omega = -100, -50, 0$ meV in the (k_x, k_y) -plane. \mathbf{q}_1 and \mathbf{q}_2 are intrapocket scattering vectors associated with the electron pockets around $(0, \pm\pi)$ and $(\pm\pi, 0)$, respectively. Intrapocket scattering vectors for the hole pockets around $(0,0)$ are not shown. \mathbf{q}_3 and \mathbf{q}_4 are the inter-pocket scattering vectors. (d-f) For most ω three parallel rod-like structures exist in the momentum space QPI, the outer peaks are positive the inner peak is negative. Since the orientation of these rod-like structures also changes near $\omega \sim -60$ meV, orientation of 1d LDOS modulation (g-i) also changes from x to y . Note: here and hereafter the momentum space plots are in the units of π/a with range $[-1, 1]$; and the real space (xy -plane) plots are in the units of a with range $[-40, 40]$. LDOS modulation shown for 80×80 size with the impurity atom located at the center, calculation done for 300×300 lattice size.

electron in the d_γ -orbital with spin σ at site i . The impurity scattering effects that generate the spatial LDOS modulations, *i.e.*, QPI patterns, are handled via a t -matrix approach on the mean field states of this theory.

Our key results are listed as the followings: (i) We obtain nearly 1d LDOS modulations, *i.e.*, real-space QPI patterns, a feature observed universally across various phases. (ii) For the five-orbital model used in this work, the wavelength of the modulations is $\sim 8a_{\text{Fe-Fe}}$ in excellent agreement with STM measurements for the SDW state of $\text{Ca}(\text{Fe}_{1-x}\text{Co}_x)_2\text{As}_2$ [7]. (iii) We identify two large energy windows of size ~ 60 meV where the LDOS modulation is one dimensional. For the SDW state it is oriented along the antiferromagnetic direction as observed in the experiment. This happens when the energy of the d_{xz} orbital is lower than that of d_{yz} . (iv) The key factor responsible for all the findings above is the OS term which leads to the upward or downward shift of either set of electron pockets located around $(0, \pm\pi)$ or $(\pm\pi, 0)$. Combined with a

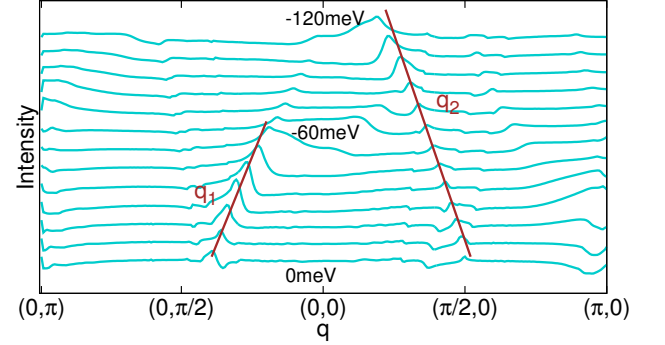


FIG. 2. QPI along the high-symmetry directions in the nematic state, for different energies, from $\omega = 0.0$ meV (bottom curve) to $\omega = -120$ meV (top curve) with energy step of 10 meV. The brown and red curves are guide to the eye for scattering vectors \mathbf{q}_1 and \mathbf{q}_2 .

large spectral density due to nearby band extrema, it results in a strongly momentum dependent spectral density along the constant energy contours, yielding the anisotropic patterns.

We start to analyze the QPI in the superconducting (SC) phase. The mean field (MF) Hamiltonian written in the Nambu formalism is

$$\mathcal{H}_{sc} = \sum_{\mathbf{k}} \Psi_{\mathbf{k}}^\dagger \begin{pmatrix} \hat{\epsilon}_{\mathbf{k}} & \hat{\Delta}_{\mathbf{k}} \\ \hat{\Delta}_{\mathbf{k}}^\dagger & -\hat{\epsilon}_{\mathbf{k}} \end{pmatrix} \Psi_{\mathbf{k}}, \quad (2)$$

where the electron field operator is defined as $\Psi_{\mathbf{k}}^\dagger = (\phi_{\mathbf{k}\uparrow}^\dagger, \phi_{-\mathbf{k}\downarrow})$ with $\phi_{\mathbf{k}\uparrow}^\dagger = (d_{\mathbf{k}1\uparrow}^\dagger, \dots, d_{\mathbf{k}5\uparrow}^\dagger)$ where subscript 1 to 5 denoting the five d orbitals $d_{3z^2-r^2}$, d_{xz} , d_{yz} , $d_{x^2-y^2}$, and d_{xy} in the same order. Here, $\hat{\epsilon}_{\mathbf{k}}$ is a 5×5 hopping matrix [34], and $\hat{\Delta}_{\mathbf{k}}$ is a 5×5 pairing matrix. Effective s^{+-} pairing state is mediated by the antiferromagnetic fluctuations generated by the interplay of Fermi surface nesting and on site Coulomb interaction, and the interaction part of the Hamiltonian is given by

$$\mathcal{H}_{int} = U \sum_{i,\mu} n_{i\mu\uparrow} n_{i\mu\downarrow} + (U' - \frac{J}{2}) \sum_{i,\mu < \nu} n_{i\mu} n_{i\nu} - 2J \sum_{i,\mu < \nu} \mathbf{S}_{i\mu} \cdot \mathbf{S}_{i\nu} + J' \sum_{i,\mu < \nu, \sigma} d_{i\mu\sigma}^\dagger d_{i\mu\bar{\sigma}}^\dagger d_{i\nu\bar{\sigma}} d_{i\nu\sigma}. \quad (3)$$

Here, the respective terms represent intraorbital, interorbital density-density, Hund's coupling and pair-hopping energy ($J' = J$) in the given order. For simplicity, we consider only intra-orbital pairing with the same and isotropic gap elements, $\Delta_0 \cos k_x \cos k_y$, (in general, the SC gap is also expected to be anisotropic [35]). We set $\Delta_0 = 20$ meV and the bandfilling is fixed at $n = 6.1$. The complete Hamiltonian is given by $\mathcal{H}_{orb} + \mathcal{H}_{sc} + \mathcal{H}_{imp}$, where $\mathcal{H}_{imp} = \sum_{\mu\sigma} V_{imp} d_{j\mu\sigma}^\dagger d_{j\mu\sigma}$ accounts for a non-magnetic delta like impurity scatterer present at site j . The modulation caused in the LDOS by the impurity term is calculated within the t -matrix approximation and only orbitally diagonal scattering is retained [36].

The MF Hamiltonian in the SDW state is obtained after

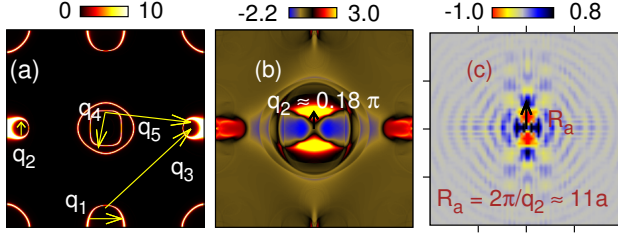


FIG. 3. Results in the s^{+-} superconducting state for $\Delta_0 = 20\text{meV}$, and quasiparticle energy $\omega = -88\text{meV}$ in the presence of orbital splitting $\delta = 60\text{meV}$: (a) Quasiparticle spectral function in (k_x, k_y) -plane, (b) Momentum space QPI in (q_x, q_y) -plane, and (c) Real-space QPI. The pockets in (a) at $(\pm\pi, 0)$ are very small with a highly anisotropic spectral density distribution along them. The intrapocket scattering vector \mathbf{q}_2 is mainly responsible for the features observed near $(0, 0)$ in the momentum-space QPI pattern. These consist of three parallel rod-like structures, the outer ones with positive peak and inner one with negative peak. Real-space QPI consists of two bright spots separated by a distance of $\sim 11a_{\text{Fe-Fe}}$ as observed in the experiments [38]. Range for all the quantities are as in Fig. 1.

standard decoupling of the on-site terms in Eq. (3) as

$$\mathcal{H}_{SDW} = \sum_{\mathbf{k}\sigma} \Psi_{\mathbf{k}\sigma}^{\dagger} \begin{pmatrix} \hat{\epsilon}_{\mathbf{k}} + \hat{N} & \text{sgn}\bar{\sigma}\hat{W} \\ \text{sgn}\bar{\sigma}\hat{W} & \hat{\epsilon}_{\mathbf{k}+\mathbf{Q}} + \hat{N} \end{pmatrix} \Psi_{\mathbf{k}\sigma}. \quad (4)$$

Here the new electron field operator is defined as $\Psi_{\mathbf{k}\sigma}^{\dagger} = (\phi_{\mathbf{k}\sigma}^{\dagger}, \phi_{\mathbf{k}+\mathbf{Q}\sigma}^{\dagger})$ with the ordering wavevector $\mathbf{Q} = (\pi, 0)$. Matrices \hat{N} and \hat{W} are obtained in a self-consistent manner. The bandfilling in this case is $n = 6.0$. We chose intraorbital Coulomb interaction $U = 0.96\text{eV}$ and Hund's coupling $J = 0.25U$ while pair-hopping interaction $J' = J$ and interorbital density-density interaction parameter $U' = U - 2J$ are determined by the standard relations. Our choice of U yields a net magnetization $m = 0.3$ consistent with the experiments [37].

Now we discuss the QPI results. Throughout, the impurity potential strength is set to be $V_{\text{imp}} = 200\text{meV}$, and the mesh size of 300×300 in the momentum space is used. Real-space QPI or LDOS modulation is obtained using the property of Fourier transform. We set the OS to be $\delta = 60\text{meV}$ unless stated otherwise. QPI in the nematic phase is calculated by setting the SC order parameters to zero with bandfilling $n = 6.0$ (for different OS values see supplementary).

To understand QPI patterns in the orthorhombic nematic or tetragonal paramagnetic phase as shown in Fig. 1(d-i), we first examine the quasiparticle spectral functions [Fig. 1(a-c)]. An important consequence of a non zero δ is the difference in size of the two sets of pockets around $(\pm\pi, 0)$ and $(0, \pm\pi)$ with large but non-uniform spectral density along both of them (see Fig. 1(a)). Note that the pockets are on the verge of disappearance near $\omega \sim -100\text{meV}$. The spectral density is larger along these pockets because of the nearby extrema. As a result, \mathbf{q}_1 and \mathbf{q}_2 are the important scattering vectors, and among them those aligned parallel to either of x - or y - directions are the most prominent ones, as they connect the regions dominated

by the same orbital. This follows straight from the fact that only intraorbital scattering is allowed. The main consequence to be described below is the orientation of LDOS modulation along either x or y .

For $\omega \sim -100\text{meV}$, \mathbf{q}_1 associated with the electron pockets around $(0, \pm\pi)$ should be the dominant scattering vector despite the fact that \mathbf{q}_2 does also connect the pockets having larger spectral density. That is because of the availability of a larger phase space as the electron pockets are bigger in contrast with those around $(\pm\pi, 0)$. In particular, \mathbf{q}_1 s which are parallel to x -direction should dominate the QPI patterns.

When energy increases through $\omega \sim -60\text{meV}$, contours of constant energies (CCEs) move away from the band extrema, and the smaller pocket around $(\pm\pi, 0)$ grows while the bigger ones around $(\pm\pi, 0)$ do not show much change. However, the spectral density along the pockets around $(\pm\pi, 0)$ becomes larger in comparison to that along the pocket around $(0, \pm\pi)$. Thus, \mathbf{q}_2 instead of \mathbf{q}_1 is now the dominant scattering vector. CCEs move further away from the band extrema, when ω increases and crosses $\sim 0\text{meV}$. Then, the QPI patterns are expected to become nearly isotropic and featureless.

As anticipated, a larger spectral density along the sides parallel to the major axis of elliptical CCEs around $(\pm\pi, 0)$ and $(0, \pm\pi)$ results in the dominance of \mathbf{q}_1 or \mathbf{q}_2 in the momentum-space QPI patterns, which is shown in Fig. 1(d-f). When $\omega < -60\text{meV}$, \mathbf{q}_1 leads to a nearly parallel rod-like positive peak structures at $\sim (\pm\pi/5, 0)$ running parallel to

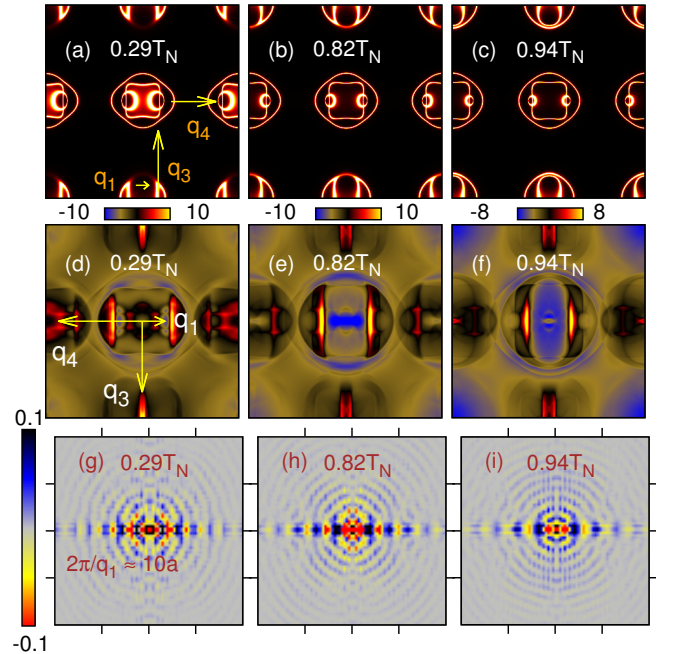


FIG. 4. Panels (a-c) show the quasiparticle spectral function for -100meV in the $(\pi, 0)$ SDW state for various temperatures. Total magnetization is $m_{\text{tot}} = 0.3$. The resulting momentum-space pattern with three parallel rod-like structures is along a direction reciprocal to ferromagnetic chain and LDOS modulation with wavelength $\sim 8 - 10a$ with the small change in temperature. Range for all the quantities are as in Fig. 1.

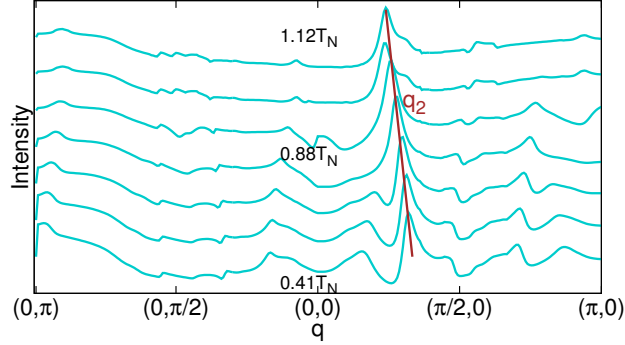


FIG. 5. QPI along the high-symmetry directions in the SDW state for different temperatures, starting from $T = 0.014t$ (bottom curve) to $T = 0.036t$ (top curve) with step of $0.04t$ ($T_N \approx 0.034t$). The brown curve is a guide to the eye for scattering vector \mathbf{q}_2 .

$q_x \sim \pm\pi/5$. A negative peak structure along $q_x \sim 0$ is also seen. When ω decreases and crosses -60meV , \mathbf{q}_2 instead of \mathbf{q}_1 becomes relevant and the patterns are rotated by 90° . Near $\omega = 0$, QPI is featureless. A recent SI-STM on $\text{FeSe}_{1-x}\text{S}_x$ does also report an isotropic QPI patterns for positive ω [39].

Figs. 1(g-i) show the real-space QPI in the immediate vicinity of the impurity atom on a 80×80 lattice size for better visibility though the calculation was done for 300×300 lattice size. Nearly 1d LDOS modulation is obtained over a wide energy window of $\sim 100\text{meV}$ centered around $\omega \approx -60\text{meV}$. As expected, modulating directions are orthogonal to each other *i.e.* along x and y for $\omega \lesssim -60\text{meV}$ and $\omega \gtrsim -60\text{meV}$, respectively. The wavelength of modulation for $\omega = -100\text{meV}$ is $\lambda_n \sim 10a_{\text{Fe-Fe}}$, which is close to $\sim 13a_{\text{Fe-Fe}}$ observed in the nematic state of NaFeAs [20]. Note that QPI dispersion shows an almost linear dependence for \mathbf{q}_1 s and \mathbf{q}_2 s, which are centered around $(0, \pi/4)$ and $(\pi/4, 0)$, respectively [Fig. 2].

Figs. 3(a,b) show calculated quasiparticle spectral function and QPI in the momentum space in the SC state for energy $\omega = -88\text{meV}$, respectively. The LDOS modulation obtained by using the Fourier transform is shown in Fig.3(c). As can be seen, a nanostructure in the vicinity of impurity atom centered around $(0, 0)$ exists with orientation along y , which can change with energy to x . The distance between two consecutive bright spots is $\sim 11a_{\text{Fe-Fe}}$. STM measurement in the SC state of $\text{FeSe}_{1-x}\text{S}_x$ with broken four-fold rotation symmetry reports scattering vector $q_x \sim \pi/8$ [39]. Similar scattering vectors have been reported earlier in FeSe as well $\text{FeSe}_{0.4}\text{Te}_{0.6}$ [38]. Thus, our results show good agreement with the experiments. Dependence of QPI pattern on the quasiparticle energy is similar in various aspects to that in the nematic state.

QPI patterns obtained for energy $\omega = -100\text{meV}$ in the SDW state as shown in Fig. 4(d-i) are the central results of this work. The dominant effect of the OS term can be easily seen even-though there is significant reconstruction of the band-structure. The band retains the salient features of nematic state and show only a little change with temperature. Consequently, the LDOS modulation is nearly 1d with orientation along the antiferromagnetic direction Figs. 4(g-i). Sim-

ilarly, the momentum-space QPI patterns consist of parallel running peak structures in a direction reciprocal to the ferromagnetic direction. An additional negative peak structure is present in between the two. All of these characteristics are in excellent agreement the STM results including a small change with the temperature. The later can be seen from the fact that there is only a little change in the scattering vector magnitude as a function of quasiparticle energy [see Fig. 5].

Similar QPI patterns have been observed in the SDW state of $\text{Ca}(\text{Fe}_{1-x}\text{Co}_x)_2\text{As}_2$ [7, 19] and NaFeAs [20]. The wavelengths for 1d LDOS modulation in the two pnictides are $\approx 8a_{\text{Fe-Fe}}$ and $\approx 13a_{\text{Fe-Fe}}$, respectively, which compares well with $\sim 8a_{\text{Fe-Fe}}$ obtained within the five-orbital of Ref. [34] considered in this work (see the TABLE I).

TABLE I. Size of one-dimensional nanostructures in the LDOS modulation of various iron-based superconductors. We obtain the length scale of the LDOS modulation $\sim 6a - 11a$.

Phase	Nematic	SDW	SC
$\text{Ca}(\text{Fe}_{1-x}\text{Co}_x)_2\text{As}_2$ [7, 19]	—	$8a$	—
NaFeAs [20]	$13a$	$13a$	—
FeSe [10, 11, 38]	—	—	$16a$

Finally, we should note that if the OS between the d_{xz} and d_{yz} orbitals is reversed ($\delta \rightarrow -\delta$), the QPI patterns in the pure SC state or in the nematic state gets rotated by $\pi/2$ for the same energy. However, its effect is nontrivial in the SDW state because it involves a significant reconstruction of the electronic structure. Also, we find that the patterns loose the 1d characteristics which is otherwise strongly favored when the orbital d_{xz} is lower in energy (see supplementary material for more details).

To conclude, the occurrence of parallel rod-like structures in the momentum space QPI or 1d spatial modulation of the LDOS in various phases of pnictides and chalcogenides is an indication of common factor at play. We identify this as a symmetry breaking term involving non degenerate d_{xz} and d_{yz} orbitals. Incorporating such a term while considering different phases, we have obtained all the essential features of QPI patterns and particularly the 1d LDOS modulations. In addition, we find it crucial that the energy of d_{xz} orbital be lower so that the orientation of anisotropic structures is robust against the change in quasiparticle energy. It is also illustrated how the non-uniform spectral-density distribution along the constant energy contours, because of the nearby band extrema, leads to highly anisotropic impurity scattering.

Acknowledgements: We are grateful to P. Wahl, S. Wirth, S. Rößler, S. Borisenko, Z. Sun, Y. Bang and I. Eremin for fruitful discussions. We acknowledge the use of HPC cluster at HRI. A.A. acknowledges support through National Research Foundation of Korea (NRF) funded by the Ministry of Science of Korea (Grants No. 2015R1C1A1A01052411 and No. 2017R1D1A1B03033465), and by the National Foundation of Korea (NRF) funded by the Ministry of Science, ICT and Fu-

-
- [1] G. R. Stewart, *Rev. Mod. Phys.* **83**, 1589 (2011).
- [2] J.-H. Chu, J. G. Analytis, K. De Greve, P. L. McMahon, Z. Islam, Y. Yamamoto, and I. R. Fisher, *Science* **329**, 824 (2010).
- [3] M. A. Tanatar, E. C. Blomberg, A. Kreyssig, M. G. Kim, N. Ni, A. Thaler, S. L. Bud'ko, P. C. Canfield, A. I. Goldman, I. I. Mazin, and R. Prozorov, *Phys. Rev. B* **81**, 184508 (2010).
- [4] E. C. Blomberg, M. A. Tanatar, R. M. Fernandes, I. I. Mazin, B. Shen, H.-H. Wen, M. D. Johannes, J. Schmalian, and R. Prozorov, *Nature Communications* **4**, 1914 (2013).
- [5] M. Nakajima, T. Liang, S. Ishida, Y. Tomioka, K. Kihou, C. H. Lee, A. Iyo, H. Eisaki, T. Kakeshita, T. Ito, and S. Uchida, *Proceedings of the National Academy of Sciences* **108**, 12238 (2011).
- [6] M. Yi, D. Lu, J.-H. Chu, J. G. Analytis, A. P. Sorini, A. F. Kemper, B. Moritz, S.-K. Mo, R. G. Moore, M. Hashimoto, W.-S. Lee, Z. Hussain, T. P. Devereaux, I. R. Fisher, and Z.-X. Shen, *Proceedings of the National Academy of Sciences* **108**, 6878 (2011).
- [7] T.-M. Chuang, M. P. Allan, J. Lee, Y. Xie, N. Ni, S. L. Bud'ko, G. S. Boebinger, P. C. Canfield, and J. C. Davis, *Science* **327**, 181 (2010).
- [8] H. Kontani, Y. Inoue, T. Saito, Y. Yamakawa, and S. Onari, *Solid State Communications* **152**, 718 (2012).
- [9] S. Kasahara, H. J. Shi, K. Hashimoto, S. Tonegawa, Y. Mizukami, T. Shibauchi, K. Sugimoto, T. Fukuda, T. Terashima, A. H. Nevidomskyy, and Y. Matsuda, *Nature* **486**, 382 (2012).
- [10] C.-L. Song, Y.-L. Wang, P. Cheng, Y.-P. Jiang, W. Li, T. Zhang, Z. Li, K. He, L. Wang, J.-F. Jia, H.-H. Hung, C. Wu, X. Ma, X. Chen, and Q.-K. Xue, *Science* **332**, 1410 (2011).
- [11] C.-L. Song, Y.-L. Wang, Y.-P. Jiang, L. Wang, K. He, X. Chen, J. E. Hoffman, X.-C. Ma, and Q.-K. Xue, *Phys. Rev. Lett.* **109**, 137004 (2012).
- [12] T. Shimojima, Y. Suzuki, T. Sonobe, A. Nakamura, M. Sakano, J. Omachi, K. Yoshioka, M. Kuwata-Gonokami, K. Ono, H. Kumigashira, A. E. Böhrer, F. Hardy, T. Wolf, C. Meingast, H. v. Löhneysen, H. Ikeda, and K. Ishizaka, *Phys. Rev. B* **90**, 121111 (2014).
- [13] K. Nakayama, Y. Miyata, G. N. Phan, T. Sato, Y. Tanabe, T. Urata, K. Tanigaki, and T. Takahashi, *Phys. Rev. Lett.* **113**, 237001 (2014).
- [14] M. D. Watson, T. K. Kim, A. A. Haghighirad, N. R. Davies, A. McCollam, A. Narayanan, S. F. Blake, Y. L. Chen, S. Ghanadzadeh, A. J. Schofield, M. Hoesch, C. Meingast, T. Wolf, and A. I. Coldea, *Phys. Rev. B* **91**, 155106 (2015).
- [15] S.-H. Baek, D. V. Efremov, J. M. Ok, J. S. Kim, J. van den Brink, and B. Büchner, *Nature Materials* **14**, 210 (2014).
- [16] P. Zhang, T. Qian, P. Richard, X. P. Wang, H. Miao, B. Q. Lv, B. B. Fu, T. Wolf, C. Meingast, X. X. Wu, Z. Q. Wang, J. P. Hu, and H. Ding, *Phys. Rev. B* **91**, 214503 (2015).
- [17] Y. Suzuki, T. Shimojima, T. Sonobe, A. Nakamura, M. Sakano, H. Tsuji, J. Omachi, K. Yoshioka, M. Kuwata-Gonokami, T. Watashige, R. Kobayashi, S. Kasahara, T. Shibauchi, Y. Matsuda, Y. Yamakawa, H. Kontani, and K. Ishizaka, *Phys. Rev. B* **92**, 205117 (2015).
- [18] J. E. Hoffman, *Reports on Progress in Physics* **74**, 124513 (2011); D. Huang, T. A. Webb, S. Fang, C.-L. Song, C.-Z. Chang, J. S. Moodera, E. Kaxiras, and J. E. Hoffman, *Phys. Rev. B* **93**, 125129 (2016); T. Hanaguri, S. Niitaka, K. Kuroki, and H. Takagi, *Science* **328**, 474 (2010); P. J. Hirschfeld, D. Altenfeld, I. Eremin, and I. I. Mazin, *Phys. Rev. B* **92**, 184513 (2015); P. O. Sprau, A. Kostin, A. Kreisel, A. E. Böhrer, V. Taufour, P. C. Canfield, S. Mukherjee, P. J. Hirschfeld, B. M. Andersen, and J. C. S. Davis, *Science* **357**, 75 (2017); J. Böker, P. A. Volkov, K. B. Efetov, and I. Eremin, *Phys. Rev. B* **96**, 014517 (2017); D. K. Singh and P. Majumdar, *ibid.* **96**, 235111 (2017); J. H. J. Martiny, A. Kreisel, P. J. Hirschfeld, and B. M. Andersen, *ibid.* **95**, 184507 (2017); D. Altenfeld, P. J. Hirschfeld, I. I. Mazin, and I. Eremin, *ibid.* **97**, 054519 (2018); B. Kamble, A. Akbari, and I. Eremin, *EPL (Europhysics Letters)* **114**, 17001 (2016); Z. Du, X. Yang, D. Altenfeld, Q. Gu, H. Yang, I. Eremin, P. J. Hirschfeld, I. I. Mazin, H. Lin, X. Zhu, and H.-H. Wen, *Nature Physics* **14**, 134 (2017); S. Choi, S. Johnston, W.-J. Jang, K. Koepf, K. Nakatsukasa, J. M. Ok, H.-J. Lee, H. W. Choi, A. T. Lee, A. Akbari, Y. K. Semertzidis, Y. Bang, J. S. Kim, and J. Lee, *Phys. Rev. Lett.* **119**, 107003 (2017); S. Sykora and P. Coleman, *Phys. Rev. B* **84**, 054501 (2011); D. K. Singh, *Physics Letters A* **381**, 2761 (2017); A. Kostin, P. O. Sprau, A. Kreisel, Y. X. Chong, A. E. Böhrer, P. C. Canfield, P. J. Hirschfeld, B. M. Andersen, and J. C. S. Davis, *Nature Materials* (2018).
- [19] M. P. Allan, T.-M. Chuang, F. Massee, Y. Xie, N. Ni, S. L. Bud'ko, G. S. Boebinger, Q. Wang, D. S. Dessau, P. C. Canfield, M. S. Golden, and J. C. Davis, *Nature Physics* **9**, 220 (2013).
- [20] E. P. Rosenthal, E. F. Andrade, C. J. Arguello, R. M. Fernandes, L. Y. Xing, X. C. Wang, C. Q. Jin, A. J. Millis, and A. N. Pasupathy, *Nature Physics* **10**, 225 (2014).
- [21] E. Bascones, B. Valenzuela, and M. J. Calderón, *Phys. Rev. B* **86**, 174508 (2012).
- [22] J. Knolle, I. Eremin, A. Akbari, and R. Moessner, *Phys. Rev. Lett.* **104**, 257001 (2010); A. Akbari, J. Knolle, I. Eremin, and R. Moessner, *Phys. Rev. B* **82**, 224506 (2010).
- [23] I. I. Mazin, S. A. J. Kimber, and D. N. Argyriou, *Phys. Rev. B* **83**, 052501 (2011).
- [24] N. Plonka, A. F. Kemper, S. Graser, A. P. Kampf, and T. P. Devereaux, *Phys. Rev. B* **88**, 174518 (2013).
- [25] H.-Y. Zhang and J.-X. Li, *Phys. Rev. B* **94**, 075153 (2016).
- [26] C. Fang, H. Yao, W.-F. Tsai, J. Hu, and S. A. Kivelson, *Phys. Rev. B* **77**, 224509 (2008).
- [27] R. M. Fernandes, A. V. Chubukov, J. Knolle, I. Eremin, and J. Schmalian, *Phys. Rev. B* **85**, 024534 (2012).
- [28] R. M. Fernandes, A. V. Chubukov, and J. Schmalian, *Nature Physics* **10**, 97 (2014); R. M. Fernandes, L. H. VanBebber, S. Bhattacharya, P. Chandra, V. Keppens, D. Mandrus, M. A. McGuire, B. C. Sales, A. S. Sefat, and J. Schmalian, *Phys. Rev. Lett.* **105**, 157003 (2010).
- [29] F. Krüger, S. Kumar, J. Zaanen, and J. van den Brink, *Phys. Rev. B* **79**, 054504 (2009).
- [30] W. Lv, J. Wu, and P. Phillips, *Phys. Rev. B* **80**, 224506 (2009); W. Lv, F. Krüger, and P. Phillips, *ibid.* **82**, 045125 (2010).
- [31] C.-C. Lee, W.-G. Yin, and W. Ku, *Phys. Rev. Lett.* **103**, 267001 (2009).
- [32] S. Onari and H. Kontani, *Phys. Rev. Lett.* **109**, 137001 (2012); H. Kontani and Y. Yamakawa, *ibid.* **113**, 047001 (2014); Y. Yamakawa, S. Onari, and H. Kontani, *Phys. Rev. X* **6**, 021032 (2016).

- (2016).
- [33] S. S. Dhesi, A. Mirone, C. De Nadaï, P. Ohresser, P. Ben-
cok, N. B. Brookes, P. Reutler, A. Revcolevschi, A. Taglia-
ferri, O. Toulemonde, and G. van der Laan, *Phys. Rev. Lett.*
92, 056403 (2004).
 - [34] H. Ikeda, R. Arita, and J. Kuneš, *Phys. Rev. B* **81**, 054502
(2010).
 - [35] X. Liu, R. Tao, M. Ren, W. Chen, Q. Yao, T. Wolf,
Y. Yan, T. Zhang, and D. Feng, *ArXiv e-prints* (2018),
arXiv:1803.07304 [cond-mat.supr-con].
 - [36] Y.-Y. Zhang, C. Fang, X. Zhou, K. Seo, W.-F. Tsai, B. A.
Bernevig, and J. Hu, *Phys. Rev. B* **80**, 094528 (2009).
 - [37] C. de la Cruz, Q. Huang, J. W. Lynn, J. Li, W. R. II, J. L.
Zarestky, H. A. Mook, G. F. Chen, J. L. Luo, N. L. Wang, and
P. Dai, *Nature* **453**, 899 (2008).
 - [38] U. R. Singh, S. C. White, S. Schmaus, V. Tsurkan, A. Loidl,
J. Deisenhofer, and P. Wahl, *Science Advances* **1**, e1500206
(2015).
 - [39] T. Hanaguri, K. Iwaya, Y. Kohsaka, T. Machida, T. Watashige,
S. Kasahara, T. Shibauchi, and Y. Matsuda, *Science Advances*
4, eaar6419 (2018).

SUPPLEMENTARY MATERIAL

1. Quasiparticle interference in the superconducting state

Modulation in the DOS due to an impurity atom is given by

$$\delta\rho(\mathbf{q}, \omega) = \frac{i}{2\pi} \sum_{\mathbf{k}} g(\mathbf{k}, \mathbf{q}, \omega), \quad (5)$$

where $g(\mathbf{k}, \mathbf{q}, \omega)$ in terms of the change in the Green's function is

$$g(\mathbf{k}, \mathbf{q}, \omega) = \sum_{i \leq 5} (\delta G^{ii}(\mathbf{k}, \mathbf{k}', \omega) - \delta G^{ii*}(\mathbf{k}', \mathbf{k}, \omega)). \quad (6)$$

Here, $\mathbf{q} = \mathbf{k} - \mathbf{k}'$. The change in the Green's function matrix due to a single non-magnetic impurity is

$$\delta \hat{G}(\mathbf{k}, \mathbf{k}', \omega) = \hat{G}^0(\mathbf{k}, \omega) \hat{T}(\omega) \hat{G}^0(\mathbf{k}', \omega), \quad (7)$$

where the meanfield Green's function is given by

$$\hat{G}^0(\mathbf{k}, \omega) = [(\omega + i\eta) \hat{\mathbf{I}} - \hat{\mathcal{H}}(\mathbf{k})]^{-1},$$

and the t-matrix is obtained as

$$\hat{T}(\omega) = (\hat{\mathbf{I}} - \hat{V} \hat{G}(\omega))^{-1} \hat{V}, \quad (8)$$

and $\hat{\mathbf{I}}$ represents a 10×10 identity matrix. Furthermore, we define

$$\hat{G}(\omega) = \frac{1}{N} \sum_{\mathbf{k}} \hat{G}^0(\mathbf{k}, \omega). \quad (9)$$

and

$$\hat{V} = V_{\text{imp}} \begin{pmatrix} \hat{\mathbf{1}} & \hat{\mathbf{O}} \\ \hat{\mathbf{O}} & -\hat{\mathbf{1}} \end{pmatrix}, \quad (10)$$

where $\hat{\mathbf{1}}$ and $\hat{\mathbf{O}}$ are the 5×5 identity matrix and null matrices, respectively. Finally, LDOS modulation or QPI in real space, $\delta\rho(\mathbf{r}, \omega)$, can be obtained by Fourier transform of $\delta\rho(\mathbf{q}, \omega)$.

2. Quasiparticle interference in the spin-density wave state

As we discussed in the main text, the MF Hamiltonian in the SDW state is obtained as

$$\mathcal{H}_{SDW} = \sum_{\mathbf{k}\sigma} \Psi'_{\mathbf{k}\sigma} \begin{pmatrix} \hat{\varepsilon}_{\mathbf{k}} + \hat{N} & \text{sgn}\bar{\sigma}\hat{W} \\ \text{sgn}\bar{\sigma}\hat{W} & \hat{\varepsilon}_{\mathbf{k}+\mathbf{Q}} + \hat{N} \end{pmatrix} \Psi'_{\mathbf{k}\sigma}. \quad (11)$$

The matrix elements of matrices, \hat{W} and \hat{N} , in the above equation are defined as

$$\begin{aligned} 2W_{\mu\mu} &= U m_{\mu\mu} + J \sum_{\mu \neq \nu} m_{\nu\nu} \\ 2W_{\mu\nu} &= J m_{\mu\nu} + (U - 2J) m_{\nu\mu} \end{aligned} \quad (12)$$

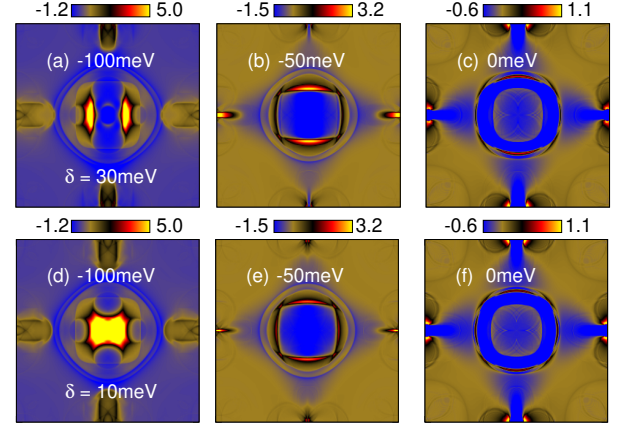


FIG. 6. Momentum-space quasiparticle interference patterns in the nematic phase with orbital-splitting $\delta = 30\text{meV}$ (first row (a), (b) and (c)) and 10meV (second row (d), (e) and (f)). Although features corresponding to one-dimensional LDOS modulation weaken on decreasing δ but still noticeable even for moderate value of $\delta = 30\text{meV}$.

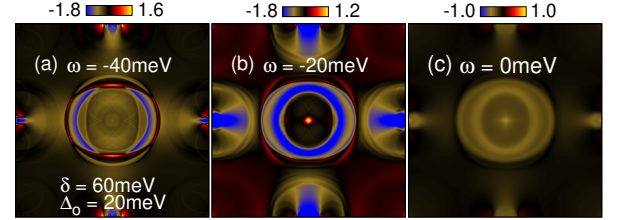


FIG. 7. Quasiparticle interference patterns in the superconducting state for $\omega = -40\text{meV}$, (b) -20meV (c) 0meV .

and

$$\begin{aligned} 2N_{\mu\mu} &= U n_{\mu\mu} + (2U - 5J) \sum_{\mu \neq \nu} n_{\nu\nu} \\ 2N_{\mu\nu} &= J n_{\mu\nu} + (4J - U) n_{\nu\mu}, \end{aligned} \quad (13)$$

where charge densities and magnetizations are given by

$$n_{\mu\nu} = \sum_{\mathbf{k}\sigma} \langle d_{\mathbf{k}\mu\sigma}^\dagger d_{\mathbf{k}\nu\sigma} \rangle, \quad m_{\mu\nu} = \sum_{\mathbf{k}\sigma} \langle d_{\mathbf{k}\bar{\mu}\sigma}^\dagger d_{\mathbf{k}\nu\sigma} \rangle. \quad (14)$$

Note that $d_{\mathbf{k}\bar{\mu}\sigma}^\dagger = d_{\mathbf{k}+\mathbf{Q}\mu\sigma}^\dagger$ with bar over orbital indices indicates shifting of momentum by $\mathbf{Q} = (\pi, 0)$. Summation over \mathbf{k} is in the first Brillouin zone.

The expressions remain similar to the case of superconducting state. However, there are several differences as well. Impurity matrix is now

$$\hat{V} = V_{\text{imp}} \begin{pmatrix} \hat{\mathbf{1}} & \hat{\mathbf{1}} \\ \hat{\mathbf{1}} & \hat{\mathbf{1}} \end{pmatrix}. \quad (15)$$

The change in the DOS is given by $\delta\rho_\alpha(\mathbf{q}, \omega)$

$$\delta\rho_\alpha(\mathbf{q}, \omega) = \frac{i}{2\pi} \sum_{\mathbf{k}} g_\alpha(\mathbf{k}, \mathbf{q}, \omega) \quad (16)$$

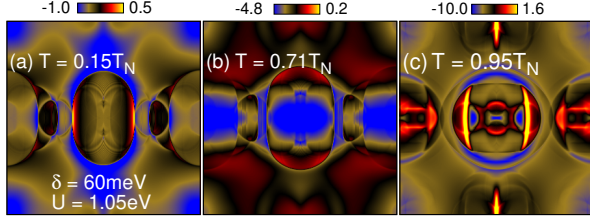


FIG. 8. Quasiparticle interference patterns in the $(\pi, 0)$ SDW state obtained for $U = 1.05\text{eV}$, $J = 0.25U$ whereas orbital-splitting $\delta = 60\text{ meV}$. Total magnetization at $T \approx 0\text{K}$ is $m \approx 0.8$.

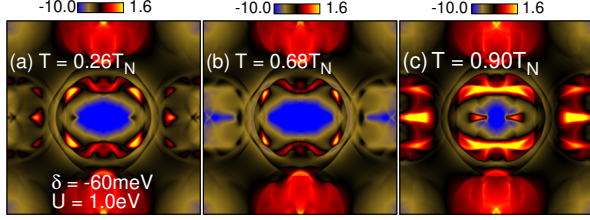


FIG. 9. Quasiparticle interference patterns in the $(\pi, 0)$ SDW state with sign of splitting reversed $\delta = -60\text{meV}$. Interaction parameter $U = 1.0\text{eV}$.

with

$$\begin{aligned}
 g_0(\mathbf{k}, \mathbf{q}, \omega) &= \text{Tr} \delta \hat{G}(\mathbf{k}, \mathbf{k}', \omega) - \text{Tr} \delta \hat{G}^*(\mathbf{k}', \mathbf{k}, \omega) \\
 g_1(\mathbf{k}, \mathbf{q}, \omega) &= \sum_{\mu \leq 5} \delta G_{\mu, \mu+5}(\mathbf{k}, \mathbf{k}', \omega) - \delta G_{\mu, \mu+5}^*(\mathbf{k}', \mathbf{k}, \omega) \\
 g_2(\mathbf{k}, \mathbf{q}, \omega) &= \sum_{\mu \leq 5} \delta G_{\mu+5, \mu}(\mathbf{k}, \mathbf{k}', \omega) - \delta G_{\mu+5, \mu}^*(\mathbf{k}', \mathbf{k}, \omega)
 \end{aligned} \tag{17}$$

and corresponding LDOS modulation is obtained as

$$\begin{aligned}
 \delta \rho(\mathbf{r}_i, \omega) &= \frac{1}{N} \sum_{\mathbf{q}} \left[\delta \rho_0(\mathbf{q}, \omega) e^{i\mathbf{q} \cdot \mathbf{r}_i} + \delta \rho_1(\mathbf{q}, \omega) e^{i(\mathbf{q}-\mathbf{Q}) \cdot \mathbf{r}_i} \right. \\
 &\quad \left. + \delta \rho_2(\mathbf{q}, \omega) e^{i(\mathbf{q}+\mathbf{Q}) \cdot \mathbf{r}_i} \right].
 \end{aligned} \tag{18}$$

We have also examined the QPI patterns in the nematic

phase for smaller value of orbital splitting δ . Although momentum space QPI features corresponding to quasi-one dimensional LDOS modulation persist even for smaller δ , it does weaken continuously on decreasing the latter (Fig. 6). This is not surprising because the asymmetry in the quasiparticle spectrum associated with the breaking of four-fold rotational symmetry decreases with δ .

Fig. 7 shows QPI patterns in the SC state. It can be clearly seen that when ω decreases and approaches $\Delta_0 = 20\text{meV}$, one dimensional characteristics declines continuously until it is lost completely when $\omega \lesssim \Delta_0$.

The QPI patterns are very sensitive to the size of the magnetic moment in the SDW state. To illustrate this, we have calculated the patterns for $U = 1.05\text{eV}$ when $\delta = 60\text{meV}$. The net magnetic moment in the self-consistently obtained SDW state is $m \approx 0.8$ for temperature close to 0K . The results are shown in Fig. 8. Features corresponding to quasi one dimensional modulation in the LDOS can be seen just below the Neel temperature T_N where the band reconstruction is insignificant and the magnetic moment is small $m \approx 0.1$. However, the same is not true for further lower temperatures such as $T \sim 0.7T_N$ or $0.15T_N$, where magnetic moments are larger $m \sim 0.6$ or 0.8 . Thus, when the magnetic exchange splitting $2\Delta \gtrsim \delta$, a complex band reconstruction perhaps yields a modification in the anisotropy in such a way that one-dimensional features are lost. Note that the magnetic moments are usually smaller than 1 in most of the pnictides [37].

Throughout the calculations, the orbital splitting was such that d_{xz} was lower in energy. We have investigated the effect of orbital splitting with sign reversed, *i.e.*, when d_{yz} orbital is lower in energy instead. The patterns in the superconducting state or in the nematic state gets rotated by 90° for the same energy if the sign of δ is reversed. This is because d_{xz} is mapped to d_{yz} by a 90° rotation. The effect, however, is non-trivial in the SDW state for the reason that the four-fold rotation symmetry is also broken by the SDW state so that d_{xz} and d_{yz} orbitals are unequally populated. Therefore, the role of additional term which removes the degeneracy of d_{xz} and d_{yz} is not itself clear. We examined the QPI patterns in the $(\pi, 0)$ SDW state with $\delta = -60\text{meV}$, where $U = 1.0\text{eV}$. Clearly, the patterns loose one-dimensional characteristics. In other words, one-dimensional QPI patterns in the SDW state with ordering wave-vector $(\pi, 0)$ is supported only when the orbital d_{xz} is lower in energy.